International Journal on Magnetic Particle Imaging
Vol 12, No 1, Suppl 1, Article ID 2603022, 3 Pages

Infinite Science Publishing

Proceedings Article

Magnetosomes: The future of theranostics?

Oliver Buchholz[a,*] · Marina Dziuba[b] · Simon Markert[b] · Dirk Schüler[b] · Ulrich G. Hofmann[c] · Serhat Ilbey[a] · Jochen Franke[a] · Frank Mickoleit[b]

[a] Bruker BioSpin GmbH & Co. KG, Ettlingen, Germany
[b] Department of Microbiology, University of Bayreuth, Bayreuth, Germany
[c] Neuroelectronic Systems, Department of Neurosurgery, Medical Center University of Freiburg, Medical Faculty, University of Freiburg, Freiburg, Germany
[*] Corresponding author, email: oliver.buchholz@bruker.com

Abstract

Magnetic nanoparticles serve as essential tracers in biomedical applications, including diagnostics such as magnetic particle imaging (MPI) and therapeutic approaches like magnetic fluid hyperthermia (MFH). However, meeting the physicochemical requirements of both applications within a single nanoparticle system remains challenging. Magnetosomes, a novel class of magnetic iron oxide nanoparticles biosynthesized by bacteria, offer a promising solution as their magnetic properties can be fine-tuned through genetic engineering. Here, magnetosomes are investigated for dual functionality as MPI tracers and MFH heat mediators, highlighting their potential as a theranostic platform.

I. Introduction

Both magnetic particle imaging (MPI) and magnetic fluid hyperthermia (MFH) rely on high-performing magnetic nanoparticles (MNPs) [1]. However, the effective integration of both applications into a combined diagnostic-therapeutic approach remains challenging [2]. Here we investigate magnetosomes, MNPs biosynthesized by magnetotactic bacteria, as promising alternative to chemically produced MNPs. Magnetosomes of the bacterium *Magnetospirillum gryphiswaldense* consist of a monocrystalline magnetite core surrounded by a biological membrane of phospholipids and specific proteins that fulfil essential functions in magnetite biomineralization [3]. Magnetosomes have unique, genetically encoded properties (e.g. high crystallinity, narrow size distribution and strong magnetization) that can be adjusted by genetic engineering [4]. In our study, we compared two types of magnetosomes (wildtype [WT] and Δ*feoAB1*) differing in their core sizes with the commercially available tracer synomag-D70 (micromod Partikeltechnologie, Germany) with respect to temperature increase induced by MFH and MPI suitability. MNPs isolated from strain Δ*feoAB1* (an iron transport mutant affected in magnetite formation) were chosen due to their enhanced magnetic particle spectroscopy (MPS) performance [5].

II. Methods and materials

The two bacterial strains yielded magnetosomes with core sizes of 33.0 ± 5.3 nm (WT) and 23.9 ± 4.8 nm (Δ*feoAB1*) (Figure 1A). MPS was performed (MPS3, Bruker BioSpin GmbH & Co. KG) with 10 µL of each MNP type (synomag: 2 mg(Fe)/mL, WT: 5 mg(Fe)/mL, Δ*feoAB1:* 2 mg(Fe)/mL; excitation frequency: 25.25 kHz for 10 s). All MPI measurements were performed on a preclinical MPI system (Bruker BioSpin GmbH & Co. KG, MPI 25/20 FF) combined with a hyperthermia insert [6]. For each particle type, a 3D system matrix was recorded prior to imaging using a 27 mm^3 cuboid sample (syno-

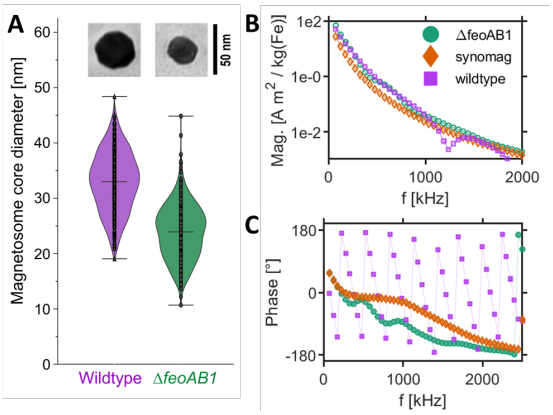

Figure 1: Core size distribution of WT and Δ*feoAB1* magnetosomes as determined from TEM micrographs ($n \geq 450$). The insets show TEM images of a representative magnetosome particle (1A). Magnetic particle spectroscopy of the different particle types (1B, C).

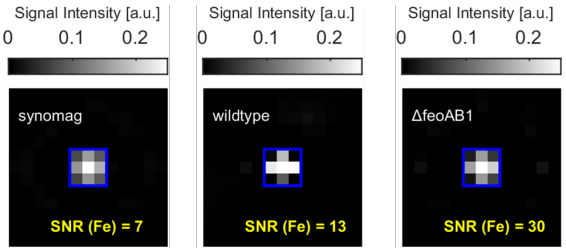

Figure 2: MPI of a cuboid sample with the different samples.

mag: 10 mg(Fe)/mL; WT & Δ*feoAB1*: analog to MPS measurements) using the following parameters: FOV = 26 × 26 × 14 mm³, pixel size = 2 mm, A = 14 mT, G = 2.5 T/m, 3 orthogonal Tx/Rx coils. The calibration samples were centered in the MPI-MFH bore. All reconstructions used a common bandwidth of 0.625 MHz, while the remaining parameters were manually defined to fit each MNP type:

Reconstruction parameter	synomag	WT	Δ*feoAB1*
Regularization (λ)	0.01	0.01	0.0001
No. iteration	3	3	20
SNR threshold	4	40	40

The image signal-to-noise ratio (SNR) was calculated as the mean signal (9-pixel ROI covering the phantom; Figure 2, blue rectangles) divided by the standard deviation of the background signal. The SNR was subsequently weighted by the respective iron concentrations. For MFH experiments, 50 µL MNP samples diluted to 2 mg(Fe)/mL and a water control were pipetted into glass tubes (Ø=6 mm). The tubes were then placed at the MPI-MFH center. The sample temperature was monitored using a thermal camera. (FLIR Systems, USA). Each MFH application comprised of 25 cycles with 24 s heating (721 kHz, 10 mT, G = 0 T/m) and 2 s pauses per cycle. Maximum temperature increases were corrected by subtracting the temperature rise of the water reference during MFH.

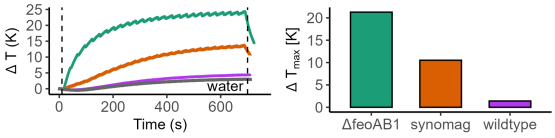

Figure 3: Temperature curves of MNP samples during MFH (left) and maximum temperature increases after control subtraction (right).

III. Results and discussion

Δ*feoAB1* magnetosomes showed the highest iron-weighted 3^{rd} harmonic magnitude (67 Am²/kg(Fe)), followed by WT (51 Am²/kg(Fe)) and synomag (27 Am²/kg(Fe)) (see Figure 1B). Magnetosomes displayed sharp magnitude decreases at higher frequencies which were absent in the synomag data. This indicates particle-particle interactions. However, the resulting differences to the synomag spectrum are minor. The WT phase showed a sharp decay over the frequency spectrum (Figure 1B), which we attribute to longer relaxation times due to the larger particle size resulting in an increased phase lag. The highest SNR was obtained for Δ*feoAB1* (30) followed by WT (13) and synomag (7) (Figure 2). Δ*feoAB1* exhibited the highest temperature increase (21.3 K), ahead of synomag (10.3 K) (Figure 3).

IV. Conclusion

Engineered Δ*feoAB1* magnetosomes provide substantially higher MFH temperature and imaging SNR than WT and synomag-D70, highlighting their strong theranostic potential.

Acknowledgments

Financial support by the European Research Council (ERC-2023-PoC, grant "BacToMagicle" to D.S.), the Federal Ministry for Economic Affairs and Energy (EXIST grant "BioMagnetix" to F.M. and M.D.), and the Bavarian FLÜGGE funding program (grant "BioMagnetix" to F.M. and M.D.) is acknowledged.

Author's statement

O.B., S.I., and J.F. are employees of Bruker BioSpin GmbH & Co. KG.

References

[1] A. Shakeri-Zadeh and J. W. Bulte, Imaging-guided precision hyperthermia with magnetic nanoparticles, *Nature Reviews Bioengineering*, vol. 3, no. 3, pp. 245–260, 2024, doi:10.1038/s44222-024-00257-3.

[2] A. Ali et al., Review on recent progress in magnetic nanoparticles: Synthesis, characterization, and diverse applications, *Frontiers in Chemistry*, vol. 9, Art. no. 629054, 2021, doi:10.3389/fchem.2021.629054.

[3] Schüler, D., Dziuba, M., Pfeiffer, D. *et al.* Biosynthesis and function of magnetic organelles in magnetotactic bacteria. *Nature Reviews Microbiology*, 2025, doi:10.1038/s41579-025-01234-2.

[4] F. Mickoleit and D. Schüler, Generation of nanomagnetic biocomposites by genetic engineering of bacterial magnetosomes, *Bioinspired, Biomimetic and Nanobiomaterials*, vol. 8, no. 1, pp. 86–98, 2019, doi:10.1680/jbibn.18.00005.

[5] F. Mickoleit et al., Development of optimized magnetic particle imaging tracers utilizing genetically engineered magnetosomes, *International Journal on Magnetic Particle Imaging*, vol. 9, no. 1, Suppl. 1, 2023, doi:10.18416/IJMPI.2023.2303066.

[6] A. Behrends, H. Wei, et al., Integrable magnetic fluid hyperthermia systems for 3D magnetic particle imaging, *Nanotheranostics*, vol. 8, no. 2, pp. 163–178, 2024, doi:10.7150/ntno.90360.